

Light Emission from the Surface of Spike-type Discharge Electrode at Negative Corona Discharge in a Non-Thermal Plasma Reactor

D. Brocilo, *Member, IEEE*, J.S. Chang, *Senior Member, IEEE*, and R.D. Findlay, *Fellow, IEEE*

Abstract—In the past, many experimental investigations for glow or streamer corona induced plasma were conducted by digital real-time or high frame-rate charge-coupled device (CCD) cameras. In this work, the light emissions observed by the CCD camera and optical spectrometers were compared and used in numerical analysis in order to determine the effect of applied voltage as well as the geometry effect in a non thermal spike-plate plasma reactor. Normalized wavelength intensities of the second positive band of nitrogen (wave length 310 to 340 nm and normally proportional to plasma density) show a symmetrical distribution around the maximum value. In contrast, the optical emission profile of the visual spectra (wave length from 400 nm blue to 700 nm red) has bimodal distribution that was also observed by a CCD camera. Therefore, the light emission from the CCD camera is not actually representative of a corona discharge or a plasma channel. Hence, all detailed investigations for any discharge plasma applications should be conducted by optical spectrometers.

Index Terms—spike-plate plasma reactor, negative corona discharge, optical spectrometer, 2nd positive band of the nitrogen molecule.

I. INTRODUCTION

THE wire-plate type geometry is a standard geometry of non-thermal plasma reactors (NTPRs) [1] and electrostatic precipitators (ESPs) [2]. In general, the NTPRs or ESPs consist of discharge and collecting electrodes. The discharge electrode is connected to the high voltage power supply either of positive or negative polarity [1], while the collecting electrode is grounded. The high electric field in the vicinity of a discharge electrode causes ionization of the gas molecules, known as a corona discharge. Ions are then moving along the electric field lines towards the collecting electrode. On their way to the collecting electrode, ions may attach to the surface

of the suspended dust particles by diffusion or field charging mechanism [2, 3]. Once charged, dust particles will be removed from the flue gases due to the introduced external electrical force in direction of collecting electrodes. When charged dust particles reach the collecting electrode, they will transfer their charge and form a dust layer. If pollutant gases are present in the flue gas, the electron, ions, and discharge generated radicals will react with pollutant gasses during oxidation or reduction processes [1].

Recent emission standards for gaseous pollutants and submicron particulate matter require development of advanced new, or modifications of existing ESP and NTPR geometries [1-3]. For example, the smooth wire-type discharge electrodes, characteristic for very low corona-onset voltage and high electric field near the discharge electrode but very frequent mechanical breakdowns, have been replaced with a more rigid type discharge electrodes such as rods and plates with needles and spikes. Additionally, the experimental studies by Parker and Hughes [4] and Howe and Houlgreave [5] have showed that the spike type discharge electrode, when oriented parallel to collecting electrodes, provide much better collection efficiency in first few metres of ESP compared to the smooth wire or rod type discharge electrodes.

Since, no comprehensive numerical and experimental validations exist for spike-plate type ESP, an investigation was conducted into the prediction of the electric field and ion density distribution as an integral part of a comprehensive study about the effect of discharge electrode geometry on charging and collection efficiency of dust particles [6]. It has been observed that the solution of the ion transport equation is very sensitive to the boundary condition at the discharge electrode surface [6, 7]. In the past, the boundary conditions of the numerical simulations for the ion transport equations were given by the continuum conditions. For example, the ion density at the surface of discharge and grounded electrode were approximately zero or order of Knudsen number (mean free path of ions/characteristic length of electrodes) [8]. However, it was difficult to use these boundary conditions, since a numerical simulation for corona discharge becomes instable due to the large ion density gradient near electrodes [18-20]. Hence, the boundary conditions near discharge and grounded electrodes were approximated by the discharge current flux near the electrodes. For a grounded electrode,

This work was supported in part by the ESTAC and NSERC.

D.B is Postdoc at McMaster University, Hamilton, Canada, (phone: 905-6280329; e-mail: drazena@power.eng.mcmaster.ca)

J.S.C. is with McMaster University Department of Engineering Physics, Hamilton, Canada, (phone: 905-5259140x24924; e-mail: changj@mcmaster.ca)

R.D.F. is with McMaster University Department of Electrical and Computer Engineering, Hamilton, Ontario, Canada L8S 4K1 (phone: 905-5259140x24874 ; e-mail: findlayr@mcmaster.ca)

surface mounted disk type current probe was used [9] to obtain the discharge current flux distributions. However, for the discharge electrode, no other experimentally obtained boundary conditions exist besides those based on the observations of light emissions by optical cameras. In this work, the boundary conditions were determined based on the experimental investigation of spectroscopic light emission near the spike-type discharge electrode. After that the experimental validations of numerical simulations of current flux near the collecting electrode wall were conducted.

II. EXPERIMENTAL APPARATUS

A schematic diagram of the experimental set-up is shown in Figure 1. Two different experiments were performed under negative corona.

The first experimental set-up was used to determine the light emitted near the discharge electrode surface by optical spectrometry and digital CCD camera systems. Normally, a digital camera or an eye can register visual wavelength spectra ranging from 400 nm (blue) to 700 nm (red), and an optical

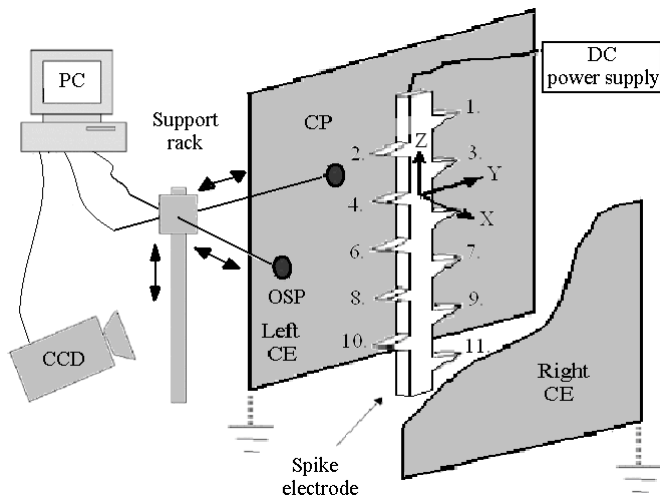


Fig. 1. Schematic diagram of the experimental set-up for measurement of light emission and current density near collecting electrode during corona discharge. (Both CE are grounded. CEs length, height, and spacing are 20, 30 and 5 cm, respectively.)

spectroscopy can measure wavelengths below 400 nm, additionally [5]. The optical spectrometry system (OCEAN OPTICS, Model PC1000) was used. The optical spectrometry probe (OSP) was connected via a single optical fibre to the spectrometer card placed in the personal computer. An optical fiber of 2 mm in diameter with SMA termination (SubMiniature version A) was used as a probe. The sampling rate of a spectrometer card was set to 1 kHz with an integration time of approximately four seconds. In order to minimize corona discharge disturbance by the OSP probe location and prevent spark-over to probe, the OSP was mounted on a rack that was placed 25 mm in front of the left collecting electrode or 111 mm from discharge electrode

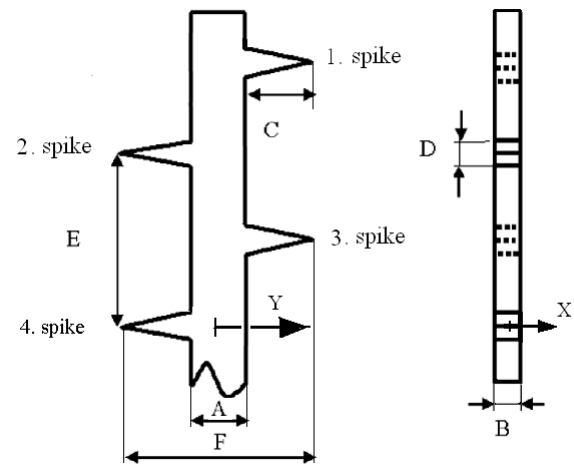


Fig. 2. Sketch of spike-type discharge electrode: (a) side and (b) front view. (Dimensions are: A=10 mm, B=1.5mm, C=D= 9 mm, E=64 mm)

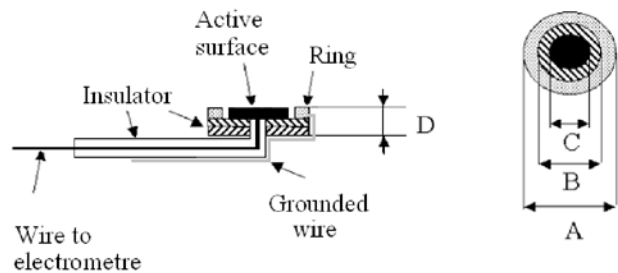


Fig. 3. Sketch of a disk-type current probe. (Dimensions are: A=6.86 mm; B=4.59 mm; C=3.33 mm; D=1 mm)

spike. The extension rods allowed for the fine positioning in X and Z directions with steps of 0.5 mm. For each (X, Z) position, five data sets were recorded. Then, the light intensity of the averaged data set was analysed and the corresponding state of gas molecules or ions were determined based on the emitted wavelengths. Additionally, the digital image of the corona discharge recorded by the CCD camera (Sony CCD-TRV) that was placed approximately one and a half metres from the discharge electrode, was compared to visible wavelengths from the optical spectrometry system to determine indirectly the spatial resolution of the optical probe. The spatial resolution of CCD system was 0.125 mm.

The second experimental set-up with disk-type current probe (CP), electro-metre, and recording device was used to measure the current density profile near the collecting electrode. The current probe schematically shown in Figure 3 was mounted on the rack and moved in (Y) and (Z) directions parallel with the surface of the left CE. For each (Y, Z) position ten data sets are recorded and averaged.

III. MEASUREMENT OF LIGHT EMISSION FROM SPIKE ELECTRODE BY OPTICAL SPECTROMETRY AND DIGITAL IMAGE ANALYSIS

During corona discharge, the spectral emission lines in air mainly originate from nitrogen molecules (N_2) [8-12]. For example, the nitrogen molecule can be transferred from the ground state $N_2(X^1\Sigma_g^+)$ into $N_2(C^3\Pi_u)$ excited state by the impact of electrons with energy greater than 11 eV. After that, the excited $N_2(C^3\Pi_u)$ molecules will transfer into $N_2(B^3\Pi_g)$ state by emitting a photon of the 337.1 nm wavelength. If electrons have an energy greater than 18.7 eV, nitrogen ions will be produced $N_2^+(B^2\Sigma_u^+)$, that will release a photons of 391.4 nm wavelength by transferring into the $N_2^+(X^2\Sigma_g^+)$ state. Typical emission spectra measured in the present system with indicated vibration levels [10-17] of N_2 second positive band (N_2 -2nd-PB) and N_2^+ first negative (N_2^+ -1st-NB) band are shown in Figure 4.

The optical intensity of various wavelengths at various voltages is shown in Figure 5. For this test, the position of the optical spectrometry probe was placed at ($X=-0.75$ mm, $Y=-125$ mm, $Z=0.5$ mm). The curves have discontinuity at -17 and -24 kV. The first discontinuity was caused by small misalignment of spike electrode due to which the corona discharge for voltages ranging from $|-8$ kV| to $|-17$ kV| occurred mainly from the spike edge that was closer to the left CE. As the magnitude of applied voltage was increased the visual observations have showed formation of the new discharge spots from edges close to the right CE. When the magnitude of negative applied voltage exceeds 24 kV, the new corona discharge spots are formed between the spikes on the main body of the electrode, having as a consequence lower spectral intensity at spike tips.

A. Optical Intensities of the Visual Band

The light emission profiles from the surface of the spike-type discharge electrode registered by CCD camera at different applied voltage are shown in Figure 6. The CCD camera detected light emission of corona discharge at an applied voltage of -10 kV, although the corona discharge onsets at approximately -7.5 kV. From -10 to -15 kV, the light emission occurs from the spike edge close to the left CE. At applied voltages from -17 to -26 kV, the light emission occurs from both edges of the spike surface. The light intensity from the left edge is higher than that from the right edge due to the electrode miss-alignment or surface tip imperfection.

Figure 7 and 8 show normalized intensity profiles of visual spectra by optical spectrometer along the various horizontal and vertical locations with respect to the 4th spike tip location. The horizontal profile at vertical location denoted as zero represents the light intensity profile along the spike tip surface. The horizontal profile denoted as 1.5 represents the profile on the line parallel with the spike tip surface at a distance of 1.5 mm. At applied voltage of -15 kV the visual band has a mono distribution with the maximum value approximately 0.6 mm to the left from the electrode center. At -22 kV, the light emission profile of visual band measured by optical spectrometer has a dual distribution with peaks at -0.7 and 0.7 mm from the electrode center.

Compared to the light intensity profile of CCD camera, the

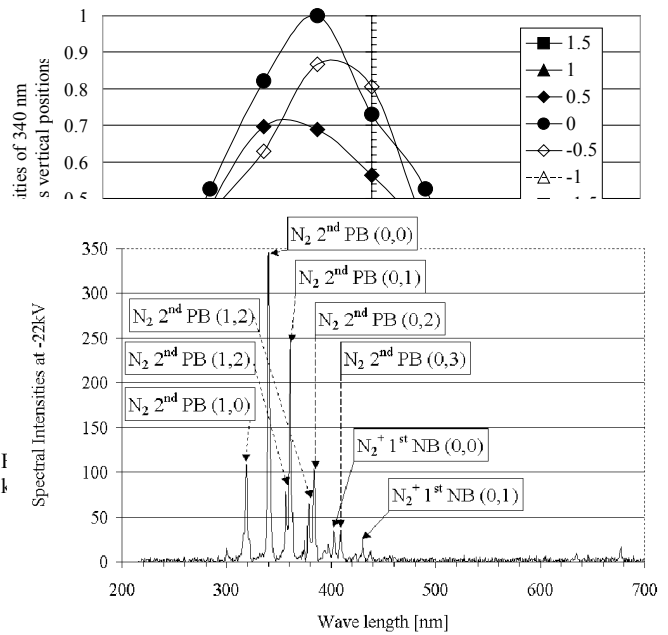


Fig. 4. Typical optical emission spectrum from center of discharge electrode surface at -22 kV.

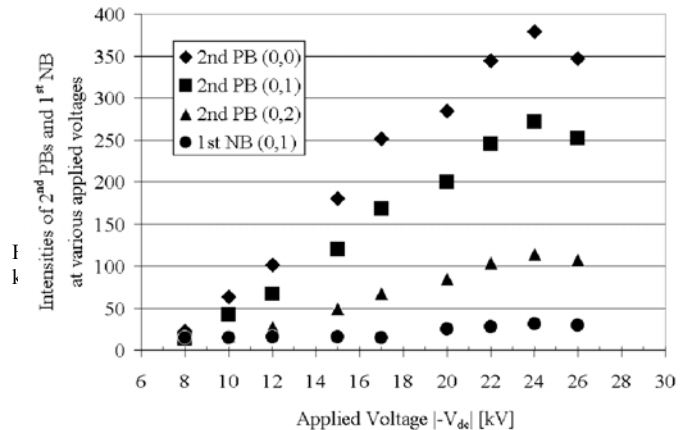


Fig. 5. Optical intensity of various wave length spectra, belonging to the 2nd PBs and 1st NB of N_2 and N_2^+ molecules at various negative applied voltages.

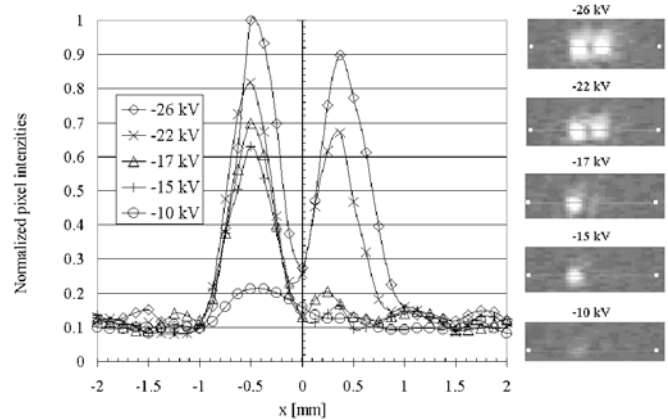


Fig. 6. Normalized pixel intensity profile of light emissions from discharge electrode surface captured by CCD camera for various applied voltages along the horizontal line passing through the centre of the 4th spike.

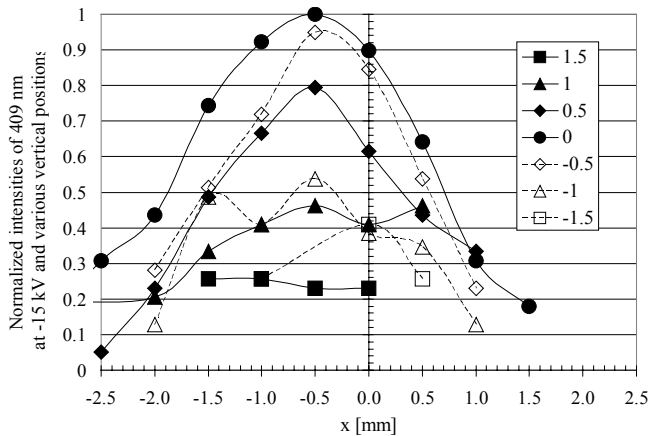


Fig. 7. Normalized spectral intensities of visual band (1st NB of N_2^+) at -15 kV for spike part of discharge electrode.

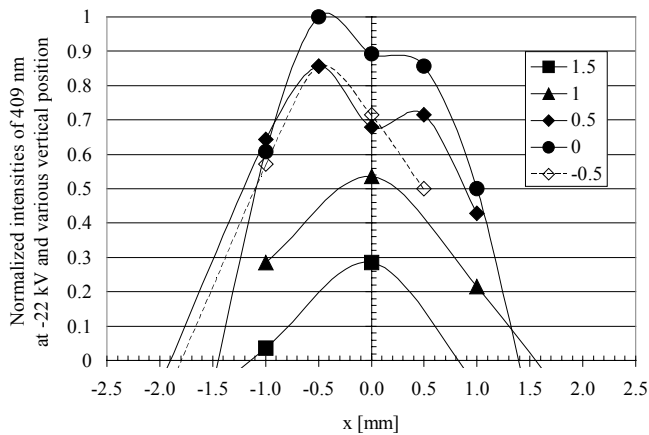


Fig. 8. Normalized spectral intensities of visual band (1st NB of N_2^+) at -22 kV for spike part of discharge electrode.

light emission profile by optical spectrometer has wider distribution and not very defined peaks. The difference is believed to be due to the spatial resolution of the optical spectrometer probe that depends on the distance between the light source and OSP, as well as the OSP size. The spatial resolution of OSP was determined indirectly. Namely, the light intensity profile by CCD camera was integrated across various diameters and compared with the profile of visual spectra from optical spectrometer. When the integration area equals the optical probe size, the integrated CCD profile was very similar to the OSS profile. This indicates that the actual light intensity profiles is narrower than that measured by optical spectrometer.

B. Optical intensities of the UV band

The horizontal profiles of the normalized wavelength intensities of 2nd positive band of N_2 (UV band) at various vertical positions with respect to the 4th spike tip location for applied voltage of -15 and -22 kV are shown in Fig. 9 and 10. Both figures show a symmetrical profile around the maximum value. The actual location of the maximum of emission intensity at -15 kV is approximately 0.5 mm shifted to the left of the centre of the electrode, similar to that of the visual band. However, the light emission profile of UV band is

narrower than the profile of the visual band. At applied voltage of -22 kV, emission profile of UV band is symmetrical with respect to the spike centre. In contrast, the visual bands has bimodal distribution.

IV. DISCUSSION AND NUMERICAL VALIDATION

The light emission of the UV band is usually associated with the electron impact of the energy greater than 11 eV and the light emission of the visual band is usually associated with the electron impact of the energy greater than of 18.7 eV. By correlating the electron energy with electric field intensity and by examining the electric field intensity near the spike tip surface, it has been observed that the electric field intensity near the edge of the spike is higher than the value in the center of the spike. Thus, around the edges of the spike ionization zone that in the present case less than 1mm or few Debye lengths, the electrons have enough energy to produce mainly the nitrogen molecule excited ions $N_2^+(B_2\Sigma_u^+)$ and low energy electron. The light emission of excited N_2^+ is small since all N_2^+ will be converted in various heavy ions before they reach the edge of the ionization zone [21]. Therefore, the visual band emission has the light intensity peaks near the spike edge location where electric field is higher. On the other hand, $N_2(C^3\Pi_u)$ excited molecules associated with lower electron energies and electric fields are produced mainly in the center of the spike. Therefore the maximum of the emission intensity of the UV band is at the center of the spike. During the electron- $N_2(X^1\Sigma_g^+)$ impact, the electron will lose most of its energy and it will be suitable for the electron attachment reaction and formation of the negative ions. Therefore, the profile of the optical emission of the UV band (2nd positive band) was used to determine the boundary conditions on the discharge electrode surface required in the calculation of the negative ion density distribution.

Multi-dimension ESP code (MESP) [6], also described in Appendix, was used to predict the ion density and electric field for the spike-plate geometry given in Fig. 1. The results were obtained for applied voltage of $V_{dc} = -22$ kV and total discharge current of 1.61 mA in still ambient air of $T = 300$ K. It was assumed that the $N_2O_2^-$ ion is a dominant negative ion [21] with the ion mobility (μ_{ni}) and ion diffusion (D_{ni}) constants of 1.577×10^{-4} [m^2/Vs] and of 3.984×10^{-6} [m^2/s], respectively. The absolute value of the electric field number $|F_E| = |eV_{dc}/kT|$ is very high ($|F_E| = 8.7 \times 10^5$), therefore the major ion transport was due to the drift of ions in electric field. The convection of ions due to the main gas flow is neglected since the mean gas velocity is zero. The electrohydrodynamically (EHD) induced secondary flow does not affect the ion transport itself, since the coupling is mainly one-way and therefore it can be neglected. The predicted current flux density near the grounded electrode was reconstructed from the numerically obtained ion density and electric field. The measured current profiles are shown in Figures 11 and 12 whereas the comparison between predicted current density profiles and the measured results at the horizontal Line 1 are shown in Figure 13.

The current profile near the collecting electrode surface reflects the complexity of the discharge electrode geometry. Due to the staggered arrangements of the spikes and their parallel orientation with respect to collecting electrode plane, the current distribution is not symmetrical with respect to the Z coordinate. Figure 11 shows the current measured along the five horizontal lines. Line 1 is aligned with the projections of the fourth spike tip. Line 5 is aligned with the projections of the symmetry line between the third and fifth spike oriented towards the ESP inlet. The measured currents are not symmetrical with respect to the central vertical line. Figure 12 shows the current profile along two vertical lines. High current densities were observed near the projection of the spike tip and low current densities were observed in the regions between spikes projections and in the region of the projection of the discharge electrode strip. The standard deviation of the measured current density is location dependant. For points located between -100 and -68 mm the standard deviation of the measured current is in the range from 1 to 2 %. For points located between -65 to -18 mm, the standard deviation is less than 1 %. The standard deviation of points between -15 and 0 mm is ranging from 10 to 31%.

The predicted current density near collecting electrode based on the UV and constant profiles of negative ion density are within 1 % difference, in spite of much larger difference in an electrode space. The current density based on the CCD profile is 5 to 17 % smaller than the previous two. Therefore, the best agreement between the measured and predicted current density is when the boundary conditions are determined based on the UV and constant profiles. Disagreement between measured and predicted current density observed at locations $-20 < Y [mm] < -15$ is due to the placement of the boundary conditions at the surface of discharge electrode instead of at the periphery of the ionization zone. At

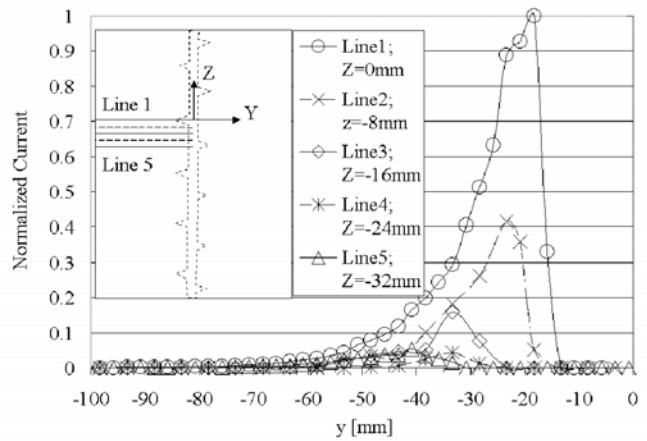


Fig. 11. Normalized current along five horizontal lines near the collecting electrode surface.

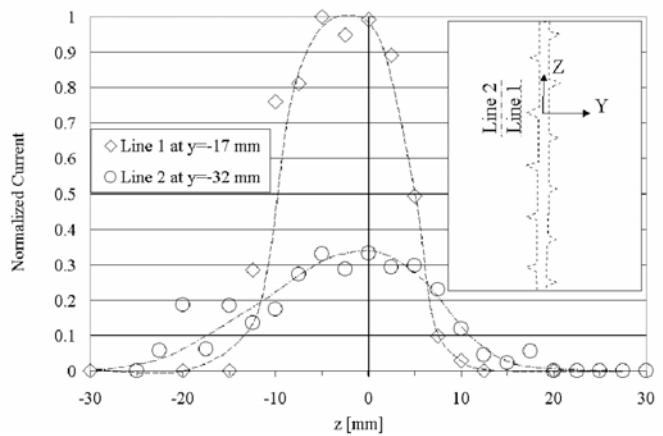


Fig. 12. Normalized current along two vertical lines near the collecting electrode surface.

present the extent of the ionization zone in Y direction could not be measured due to the shade of the structure that holds the discharge electrodes. In the region from $-15 < Y [mm] < 0$ the disagreement between experimental and predicted values is caused by the coarse grid mapping of the region, which requires further improvement.

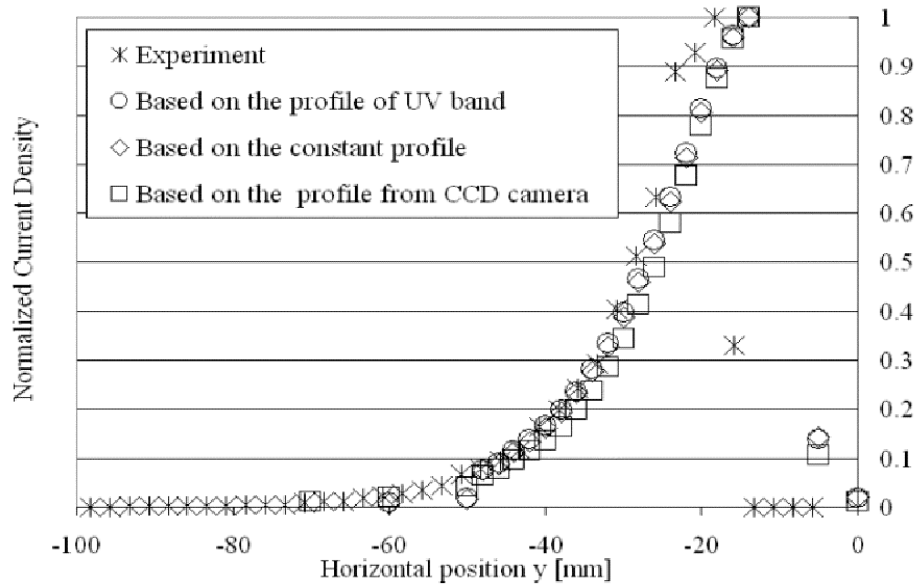


Fig. 13. Normalized current along horizontal Line1 at X=-25 mm and Z=0mm.

V. CONCLUSION

Based on the experimental and numerical results, the following concluding remarks were obtained:

- 1) Experimental results show almost a linear increase of spectral intensity with an increase of modulus of applied voltage up to $|-24 \text{ kV}|$, after which the intensity decreases. The visual observations have showed that the new corona discharge spots are formed at the main body of the electrode in the area between the spikes when the magnitude of negative applied voltage exceeds 24 kV. Hence, the spectral intensities at spike tip diminish.
- 2) Normalized wavelength intensities of the second positive band of nitrogen show a symmetrical profile around the maximum value for applied voltages of -22 kV. In contrast, the optical emission profile of the visual spectra at -22 kV has bimodal distribution. Similar profile of the visual spectra was also observed by a CCD camera.
- 3) Comparison of measured and predicted current density near collecting electrode showed the best agreement when boundary conditions on the surface of spike electrode were based on the second positive band or constant profiles rather than on the profile obtained only by a CCD camera.
- 4) The light emission from the CCD camera is not actually representative of a corona discharge or a plasma channel. Hence, all detailed investigations for any discharge plasma applications must be by optical spectrometers.

ACKNOWLEDGMENT

This work was supported in part by the ESTAC and NSERC. Authors thank to Dr. S. Ono for discussions and comments.

REFERENCES

- [1] K. Urashima and J.S. Chang, "Removal of volatile organic compounds from air streams and industrial flue gases by non-thermal plasma technology," *IEEE Transactions on Dielectrics and Electrical Insulation*, vol. 7, no. 5, Oct. 2000, pp. 602-614.
- [2] A. Mizuno, "Electrostatic precipitation," *IEEE Transactions on Dielectrics and Electrical Insulation*, vol. 7, no. 5, Oct. 2000, pp. 615-624.
- [3] S. Masuda and S. Hosakawa, "Electrostatic Precipitation," in *Handbook of Electrostatic Processes*, Marcel Dekker, Inc., 1995, Chapter 21.
- [4] K. R. Parker and G. Hughes, "A visual investigation of corona induced turbulence in a laboratory scale model precipitator," in *Proceedings of the Third International Conference on Electrostatic Precipitation*, Padova, Italy, October 1987, pp. 379-399.
- [5] A.F. Howe and J. Houlgreave, "An experimental investigation of the charging of different sized particles in a precipitator," in *Proceedings of the Third International Conference on Electrostatic Precipitation*, Padova, Italy, October, 1987, pp. 329-336.
- [6] D. Brocilo, J.S. Chang, and R.D. Findlay, "Modeling of electrode geometry effects on dust collection efficiency of wire-plate electrostatic precipitators," *Proceedings, 8th international conference on Electrostatic Precipitation*, May 2001, vol. II, A4-3.
- [7] R. G. Corbin, "Electrical performance of serrated strip electrodes in electrical precipitators," in *Proceedings of the Third International Conference on Electrostatic Precipitation*, Padova, Italy, October, 1987, pp. 843-855.
- [8] A.A. Yastrebov, "Theory of the spectral probe in a dense plasma," *Soviet Phys.-Tech. Phys.*, Vol. 17, pp. 638-645, 1972.
- [9] Y. Kondo and Y. Mixoshi, "Pulseless corona in negative point to plane gap," *Japanese J. Appl. Phys.*, vol. 17, pp. 643-649, 1978.
- [10] Y. Kim, S.H. Hong, M.S. Cha, Y.H. Song, and S.J. Kim, "Measurement of electron energy by emission spectroscopy in pulsed corona and dielectric barrier discharges," *Journal of Adv. Oxid. Technology*, vol. 6, no. 1, pp. 11-16, 2003.
- [11] S. Ono and S. Teii, "Vibrational temperature in a weakly ionized steady-state nitrogen discharge plasma," *J. Phys. D. Appl. Phys.*, vol. 16, pp. 163-170, 1983.
- [12] Y. Uchida, K. Takaki, K. Urashima, and J.S. Chang, "Atmospheric pressure nitrogen plasma in a ferro-electric packed bed barrier discharge, Part II," *IEEE Transaction on Dielectrics and Electrical Insulation*, (In Press 2003).
- [13] N. Ikuta, K. Kondo, "A spectroscopic study of positive and negative coronas in $\text{N}_2 \text{O}_2$ mixture," *Proceedings of 4th International Conference on Gas Discharges and Their Applications*, Swansea, UK, 1976, pp. 227-230.

- [14] S.V. Pancheshnyi, S.M. Starikovskaia, and A.Yu. Starikovskii, "Collisional deactivation of $N_2(C^3\Pi_u, =0, 1, 2, 3)$ states by N_2, O_2, H_2 and H_2O molecules," *Chemical Physics*, vol. 262, pp. 349-357.
- [15] W.S. Struve, *Fundamentals of Molecular Spectroscopy*. New York-Wiley, 1989.
- [16] G. Herzberg, *Molecular Spectra and Molecular Structure*. New York, Prentice-Hall, 1939.
- [17] R. W. B. Pearse and A. G. Gaydon, *The Identification of Molecular Spectra*. Chapman and Hall, London, 4th edition, 1976.
- [18] I. Gallimberti, "Recent advancements in the physical modeling of electrostatic precipitators," *Journal of Electrostatics*, vol. 43, pp. 219-249, 1988.
- [19] A.A. Kulikovskiy, "Production of chemically active species in the air by a single positive streamer in a nonuniform field," *IEEE Transaction on Plasma Science*, vol. 25, no. 3, pp. 439-446, June 1997
- [20] T. Yamamoto and H. R. Velkoff, "Electrohydrodynamics in an electrostatic precipitator," *J. Fluid Mech.*, vol. 108, pp. 1-18, 1981.
- [21] J. S. Chang and A. Kwan, "Modeling of dry air chemistry in a coaxial wire-pipe negative corona discharge," *ESA-IEJ Joint Symposium on Electrostatics 1998 Proceedings*, Press Morgan Hill, California, June 1998, pp. 390-407.
- [22] J.S. Chang, M. Kamitsuma and J.G. Laframboise, "Streamline Curvature Up-Wind Difference Method for Modelling of Steady heat, Mass and Plasma Transfer to Cylinder in Cross-Flow," in *Proc. Int. Conf. Comp. Fluid Dynamics*, K. Oshima, Ed. vol. 1, pp. 422-434.

APPENDIX

NUMERICAL MODEL

Detailed description of the model can be found in Ref. [6]. For completeness, a short description of numerical model is introduced in this appendix as follows. The high spectral intensity of the N_2 -2nd-PB together with spectral intensity of the N_2^+ -1st-NB bands can be used to reconstruct the mean density (N) of excited molecules in discharge from Eq. 1.

$$N \propto \frac{I}{N_e \int_0^{\infty} \sigma(\varepsilon) \cdot f(\varepsilon, T_e) \cdot v(\varepsilon) \cdot d\varepsilon} = \frac{I}{N_e \cdot \alpha} \quad (1)$$

Here, I is the optical intensity, N_e is the electron density, $\sigma(\varepsilon)$ is the cross section of reactions, $f(\varepsilon, T_e)$ is the electron energy distribution, $v(\varepsilon)$ is the electron velocity, ε is the electron energy, T_e is the electron temperature and α is the reaction rate coefficient [10]. This approach would require the modeling of the complex corona chemistry [19, 21]. In this work, the problem was simplified by assuming that from the edge of ionization region only ionic current consisting of negative ions is injected in an inter-electrode space [14]. Positive ions and electrons, found in a corona-glow zone near a discharge electrode, are not considered as a consequence of by-passing of corona chemistry and a fact that the corona-glow zone is normally very thin (within few Debye lengths and less than 1mm in present case). Only, the normalized profile of the measured optical intensity has been used to set the boundary conditions for negative ions at the discharge electrode. In order to validate the boundary condition the multi-dimension ESP code (MESP) [13] has been developed that allows for the comparison between predicted and measured current densities near collecting electrode.

The MESP code, consisting of three sections as shown in Figure 14. The first section labeled as ESP geometry and operating parameters involves the selection of: (a) collecting and discharge electrode dimensions, (b) magnitude of dc applied voltage, (c) operating main gas parameters such as: flow rate, gas composition, and temperature. After that, the program proceeds with initial calculations, that include analytic approximations for the main gas flow, Laplace's electric field, and guessed number of initial ions (N_{i0g}) based on electric field on the surface of discharge electrode, and

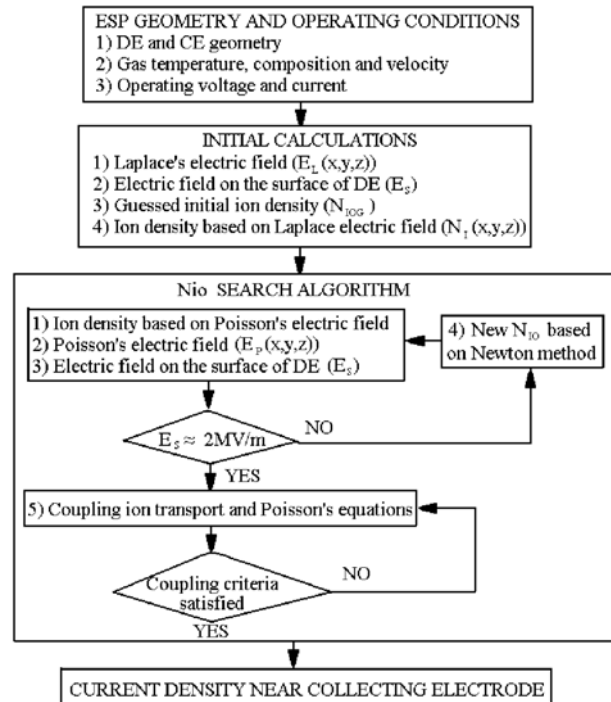


Fig. 14. Block diagram of the MESP code.

predicted averaged current from current-voltage (I-V) model. The next section labeled as N_{i0} search algorithm is based on the Newton method and it couples ion transport and Poisson's electric field equations in iterative way until the critical electric field (approx. 2 MV/m) near the discharge electrode surface was reached. After that the Poisson's and ion transport equations with N_{i0} value from the search algorithm together with a boundary conditions based on a measured light emission from spike surface were coupled in an iterative way until the solutions were self-consistent. The whole procedure can be time consuming, especially for three dimensional studies, therefore the estimate of the first initial N_{i0} value is quite critical. The last section of MESP code calculates the current density profile near the collecting electrode and total discharge current delivered to the collecting electrodes.

A. Ion Density

In general, the spike electrode creates complex electric field and ion density distribution in an inter-electrode spaces [6]. Additionally, the ion density distribution, obtained from the ion transport equation, is highly affected by the boundary

conditions on the discharge electrode surface. The ion density calculations were based on the steady-state frozen chemistry ion transport equation for three dimensional domain. The dimensionless form of the equation for the case of negative ions, constant ion mobility (μ_{ni}) and ion diffusion (D_{ni}), chemistry with balanced source and sink term ($S_{ni} - R_{ni}=0$) is shown in (2a). The production and loss of negative ions due to the electron attachment, detachment or positive ion recombination is considered zero outside the ionization zone,

$$Ra_i \bar{u}_g \cdot \tilde{\nabla} n_{ni} - F_E n_{ni} \tilde{\nabla} \cdot \bar{\xi} - F_E \bar{\xi} \cdot \tilde{\nabla} n_{ni} - \tilde{\nabla}^2 n_{ni} = S_{ni} - R_{ni} \quad (2a)$$

$$Ra_i = U_0 L / D_{ni} \quad ; \quad F_E = eV_0 / (kT) \quad (2b)$$

where $\tilde{\nabla} = L\nabla$ is dimensionless operator, L [m] is the characteristic length, Ra_i is the dimensionless diffusion Reynolds number, F_E is dimensionless electric field number, $u_g = U_g/U_0$ is the dimensionless gas velocity, U_0 [m/s] is the mean gas velocity, $n_i = N_i/N_{i0}$ is the ion number density ratio, N_{i0} [# of ions/m³] is the initial number density of ions, $\bar{\xi} = -\tilde{\nabla}\Phi^*$ is the dimensionless electric field, V_0 [V] is the applied voltage, D_{ni} [m²/s] is the ion diffusion, L [m] is the characteristic length, $e=1.602 \times 10^{-19}$ [C] is the charge of one electron, $k=1.381 \times 10^{-23}$ [J/K] is the Boltzmann constant, T [K] is the gas temperature. The ion mobility (μ_{ni}) is considered to be invariant to the electric field and is correlated with ion diffusion (D_{ni}) over Einstein's relation ($\mu_{ni} = D_{ni}e/kT$).

With respect to the boundary conditions, the normalized profile of the optical emission of the 2nd positive band of N₂ molecules that is directly proportional to the electron density and hence proportional to the negative ion distribution, was used to set the boundary condition near the discharge electrode surface. The profiling function A_f obtained by fitting to the experimental data is shown in dimensionless form (3),

$$A_f(x') = -0.4366(x')^2 + 1 \quad (3)$$

where $x'=x/B$ is the normalized horizontal position with respect to the length of the spike tip (B) ($-0.5 \leq x' \leq 0.5$). Locations of discharges in the axial direction is determined by spike tip positions. In addition to the boundary conditions based on the profile of the 2nd positive band, Gaussian-like distribution that covers the whole surface of the spikes, two other conditions were tested. These are: (a) based on the profile obtained by CCD camera, that looks like a bimodal distribution with the peaks at the edges of the spikes, and (b) based on the assumption of the constant ion density along the whole surface of the spike tip. The boundary condition at collecting electrode is set to zero. The ion density gradient in the direction normal to the inlet, outlet, bottom and top planes of the ESP is set to zero ion density.

Equation (2a) is of the steady-state quasilinear second-order elliptic partial differential equation of convection-diffusion type and its solution depends on the Ra_i and F_E ratio. For considerable ion drift ($|F_E| \gg Ra_i$), the value of n_{ni} remains very close to the conditions at discharge electrode. The upwind differencing method [22], for which the value at the

interface is equal to the value at the grid point on the upwind side, is the well-known approach used for the formulation of terms containing ∇n_{ni} . The second term that contains the ($\nabla \cdot \bar{\xi}$) is usually substituted by Poisson's equation (4a). Central differencing method is used for the fourth term.

B. Electric Potential

The electric potential is obtained from the Poisson's equation (4a) written in dimensionless form,

$$\tilde{\nabla}^2 \Phi^* = -Db_i^* n_i \quad (3.11f)(4a)$$

$$Db_i^* = Db_i^2 / F_E \quad ; \quad Db_i = L / \lambda_{Di} \quad (4b)$$

$$\lambda_{Di} = \sqrt{\epsilon kT / e^2 N_{i0}} \quad (4c)$$

where the $\Phi^* = \Phi/\Phi_0$ is the dimensionless electric potential ratio, $\Phi_0 = F_E = eV_0/(kT)$ is the electric field number, Db^* is Debye (Db) versus electric field number (F_E) ratio, λ_D [m] is Debye length, $n_i = N_i/N_{i0}$ is the dimensionless number of negative ions, N_{i0} [# /m³] is the initial number of ions $\epsilon = 8.854 \times 10^{-12}$ [F/m] is the electrical permittivity of free space, $e = 1.602 \times 10^{-19}$ [C] is the charge of one electron, V_0 [V] is the applied voltage, $k = 1.381 \times 10^{-23}$ [J/K] is the Boltzmann constant, T [K] is the gas temperature.

The boundary conditions for electric potential are: (a) $\Phi^* = 0$ at the collecting electrodes, (b) $\Phi^* = 1$ at corona discharge electrode, and (c) the voltage gradient in the direction normal to the boundary at the inlet, outlet, bottom, and top plane of the ESP is zero.

Equation (4a) can be classified as a second-order partial differential equation of elliptic type, whose solution for spike-plate geometry was obtained by finite difference method.

The current density \bar{J} [A/m²] near collecting electrode is reconstructed from and according to Eq. 5.

$$\bar{J} = \frac{eN_{i0}D_{ni}}{L} (Ra_i \bar{u}_g n_{ni} - F_E n_{ni} \bar{\xi} - \tilde{\nabla} n_{ni}) \quad (5)$$